

See discussions, stats, and author profiles for this publication at: <https://www.researchgate.net/publication/231647709>

High Aspect Ratio Ternary Zn_{1-x}Cd_xO Nanowires by Electrodeposition for Light-Emitting Diode Applications

ARTICLE in THE JOURNAL OF PHYSICAL CHEMISTRY C · JULY 2011

Impact Factor: 4.77 · DOI: 10.1021/jp202608e

CITATIONS

38

READS

4

5 AUTHORS, INCLUDING:



Lupan Oleg

University of Central Florida

136 PUBLICATIONS 3,587 CITATIONS

[SEE PROFILE](#)



Thierry Pauperté

Chimie ParisTech

163 PUBLICATIONS 4,738 CITATIONS

[SEE PROFILE](#)



Tangui Le Bahers

Claude Bernard University Lyon 1

33 PUBLICATIONS 867 CITATIONS

[SEE PROFILE](#)



Bruno Viana

École nationale supérieure de chimie de Paris

386 PUBLICATIONS 5,592 CITATIONS

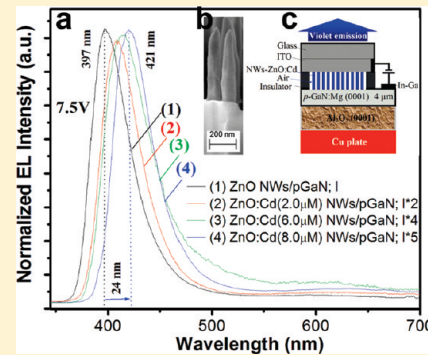
[SEE PROFILE](#)

High Aspect Ratio Ternary $Zn_{1-x}Cd_xO$ Nanowires by Electrodeposition for Light-Emitting Diode Applications

Oleg Lupon,^{†,§} Thierry Pauporté,^{*,†} Tangui Le Bahers,[†] Ilaria Ciofini,[†] and Bruno Viana[‡][†]Laboratoire d'Electrochimie, Chimie des Interfaces et Modélisation pour l'Energie (LECIME), UMR 7575 CNRS, Chimie ParisTech, 11 rue P. et M. Curie, 75231 Paris cedex 05, France.[‡]Laboratoire de Chimie de la Matière Condensée de Paris, UMR 7574-CNRS-ENSCP-UPMC, 11 rue P. et M. Curie, 75005 Paris, France.

Supporting Information

ABSTRACT: We present a combined experimental and computational approach to study $Zn_{1-x}Cd_xO$ nanowires (NWs) and their integration in light-emitting diode (LED) structures. Self-standing $Zn_{1-x}Cd_xO$ NWs have been electrodeposited on fluorine-doped tin oxide and p-GaN substrates. The electrochemical behavior has been studied, and the reaction mechanism is discussed. Low-dimensional $Zn_{1-x}Cd_xO$ structures have been obtained for $CdCl_2$ concentrations in the deposition bath lower than $6\ \mu M$ whereas at higher concentration it is admixed with crystallized CdO and the aspect ratio of the wires is decreased. According to scanning electron microscopy observations, the $Zn_{1-x}Cd_xO$ NWs have a higher aspect ratio (>30) than pure ZnO NWs (~ 20) grown in similar conditions. Analyses show that the ZnO is doped with cadmium incorporated within ZnO NWs and that Cd doping increases with increasing Cd(II) content in the deposition bath. X-ray diffraction studies show increased lattice parameters in Cd-alloyed ZnO NWs. Photoluminescence studies on pure ZnO and $Zn_{1-x}Cd_xO$ NWs show the near band-edge emission red shifted by 3–7 nm as a function of Cd(II) concentration (4 or $8\ \mu M$ in the electrolyte). The structural and optical properties of the prepared $Zn_{1-x}Cd_xO$ materials have been interpreted using density functional theory (DFT) to computationally simulate the effect of Cd substitution for Zn in the ZnO lattice. DFT calculations show that the crystal lattice parameters increase with the partial replacement of Zn atoms by Cd and that the band gap enlargement is due to the increased lattice parameters. We demonstrate the possibility to tailor the electroluminescence emission wavelength by cadmium doping in ZnO nanowires integrated in $Zn_{1-x}Cd_xO$ NWs/p-GaN heterojunction based LED structures. Reported results are of great interest for the research on band gap engineering of low-dimensional zinc oxide by doping/alloying NWs and for wavelength-tunable LED applications.



1. INTRODUCTION

Zinc oxide (ZnO) has attracted great research interest due to its wide and direct band gap (3.37 eV), large exciton binding energy (60 meV), diverse groups of nanoarchitectures, and versatile physicochemical properties.¹ During the past decade, ZnO nanowires (NWs) and nanorods (NRs) with superior properties compared to bulk material have been reported extensively. It has generated great interest due to the importance of dimensionality, high crystalline quality, large aspect ratio, and quantum confinement effects. These effects are more evident in sub-100-nm structures² with high aspect ratio and favor the study of new quantum-mechanical phenomena and development of multifunctional nanodevices. Smaller-diameter ZnO NWs are expected to lower the lasing threshold,³ to decrease the defect density at interfaces, and to increase the optical power extraction of the light-emitting diodes (LEDs).⁴ Synthesis and characterization of ZnO nanostructures has been reported extensively. Recently, integration of ZnO NRs/NWs in nanosensors, dye-sensitized solar cells, light-emitting devices, photodetectors, and

nanogenerators has confirmed their multifunctional character.^{5–12} Control and tuning properties of nano-ZnO to achieve a specific functionality have become an important field of research. One important step is to control doping and alloying effects in zinc oxide at the nanoscale and controlled doping can tailor the properties of ZnO to specific applications. For ZnO, it is essential to understand the effects of anionic or cationic substitutions and their impact on the electronic and optical properties.¹³ Modulation and engineering of the band gap in the growth direction are important for the fabrication of heterostructures. The ternary systems $Zn_{1-x}Cd_xO$ and $Zn_{1-y}Mg_yO$ permit a decrease or increase, respectively, in the band gap energy, in comparison with binary host material ZnO.^{13,14} However, a technology tool with controlled regimes has to be developed for the synthesis of doped nano-ZnO, which will permit state-of-the-art, cost-effective,

Received: March 19, 2011

Revised: June 7, 2011

Published: June 22, 2011

bottom-up synthesis technologies for nanoelectronics. We will focus here on alloying ZnO by cationic substitution with cadmium (Cd) and new inputs.

Cd and Zn belong to group IIb of the periodic table and possess similar physical and chemical properties due to similar valence electron structure. Cadmium oxide is a cubic-structure semiconductor material with band gap energy of 2.3 eV and high electrical conductivity. Cd-dopant in ZnO is considered as one of the most promising candidates for narrowing the band gap energy of zinc oxide.^{13,14} Since the ionic radius of Cd²⁺ ($\sim 0.92 \text{ \AA}$) is different than of Zn²⁺ ($\sim 0.74 \text{ \AA}$), the stable ZnO wurtzite phase is expected to be conserved only for rather low concentration of cadmium in the host oxide.¹⁴ Such properties indicate that Cd could be incorporated into ZnO to be used for band gap tuning/engineering, which could be useful for device applications.^{13,14} Thus, ZnO doping with Cd theoretically permits band gap narrowing and wavelength tunability to blue or even green light spectra range.

Several techniques such as thermal evaporation, chemical vapor deposition, thermolysis, chemical bath deposition, spray pyrolysis, and electrochemical deposition have been employed to fabricate Cd–ZnO material.^{15–23} Among the growth deposition techniques of Zn_{1-x}Cd_xO, electrochemical deposition is a powerful approach with huge potential for industrialization due to its simplicity, cost-efficiency, reproducibility, large-area deposition, low synthesis temperature, and good-quality nanomaterial.^{6–9,18} Moreover, electrochemical deposition allows mixing of the chemicals at the atomic level, thus reducing the possibility of secondary phase formation.

It is of importance to mention that, up to now, there have been few experimental studies on the properties of Cd-alloyed ZnO films grown by the electrochemical method,^{20–24} and to the best of our knowledge, there is only one report on the synthesis of Zn_{1-x}Cd_xO nanorods.²¹ Tortosa et al.²² obtained ternary single phase Zn_{1-x}Cd_xO alloy semiconductor films by a cost-effective electrodeposition method onto conductive glass substrates. They observed a controlled red shift of the optical gap with an increase in the amount of Cd present in Zn_{1-x}Cd_xO films. Mari et al.²³ synthesized ZnCdO thin films by electrodeposition and reported on the influence of the Cd content on structural, electrical, and optical properties of the ZnCdO layers. Experimental results by Mari et al.²³ demonstrated that the electrodeposition technique is effective to obtain ternary ZnCdO films (with Cd content between 1% and 9%) hexagonal ZnO phase. Li et al.²¹ reported the electrochemical preparation of Zn_{1-x}Cd_xO nanorods forming aggregates on a Cu substrate with controlled optical properties and with adjustable band gap by changing Cd content between 0 and 15%.

However, several issues have to be clarified, such as controlling Cd alloying of ZnO nanowires and simultaneously maintaining their self-standing one-dimensional morphology and high-aspect ratio. This is important because nanowire light emitters act as a waveguide and favor light extraction from potential devices. Moreover, we can expect that thin wires with high aspect ratios will enhance light extraction. Another important issue is the ability to tune the chemical and physical properties of ternary nanomaterial by incorporation of cadmium into the ZnO lattice. The addition of Cd in ZnO NWs can permit band gap engineering¹⁴ to create barrier layers and quantum wells which will facilitate radiative recombination by carrier confinement.²⁴ Thus, ZnO/p-GaN and Zn_{1-x}Cd_xO/ZnO junctions, which are key elements in zinc oxide based light emitters and detector can be fabricated. To the best of our knowledge, neither high-aspect

ratio, high quality, Zn_{1-x}Cd_xO nanowire arrays by electrodeposition nor the effect of Cd content on their properties have been reported in the literature before.

In this work, an electrochemical synthesis procedure for Zn_{1-x}Cd_xO NWs with high-aspect ratio well-tailored to LED application was found. Structural and optical properties were studied and described. A Zn_{1-x}Cd_xO NWs growth mechanism is suggested based on experimental observations. LED device structures based on n-Zn_{1-x}Cd_xO/p-GaN heterojunction with tunable emission wavelength are presented to illustrate a potential application. The structural and optical properties of the prepared Zn_{1-x}Cd_xO material has been interpreted by using a density functional theory (DFT) approach to study the effects of Cd doping by the replacement of Zn atoms in the crystal lattice.

2. EXPERIMENTAL SECTION

2.1. Electrodeposition. Electrodeposition (ECD) of pure ZnO and Zn_{1-x}Cd_xO NWs was performed in a classical three-electrode electrochemical cell.^{25,26} A deionized (DI) water (18.2 MΩ·cm) based solution containing 0.2 mM ZnCl₂, 0.1 M KCl as supporting electrolyte, and continuous bubbling of oxygen in a bath solution was used. The CdCl₂ (Alfa Aesar) was added to the electrolyte in a large concentration range, between 0 and 100 μM. The initial pH of the solutions was 5.5. The three-electrode electrochemical cell was mounted in a thermo-regulated bath. The electrolyte was saturated with pure oxygen by bubbling for 45 min prior to starting the electrolysis, and the bubbling was continuously maintained during the growth process. The substrates were glass sheets coated with F-doped SnO₂ (FTO) polycrystalline films with a sheet resistance of 10 Ω/sq. Before electrodeposition the FTO substrates were cleaned sequentially in acetone and then ethanol (95%) for 6 min each in an ultrasonic bath, followed by rinsing with flowing DI water (18.2 MΩ·cm). Afterward, these substrates were immersed in HNO₃ (45%) for 2 min and finally rinsed in DI water for 5 min in an ultrasonic bath. Once the conducting FTO substrate was cleaned and dried in flowing air, it was mounted on the working electrode (WE) for electrochemical deposition. The reference electrode (RE) was a saturated calomel electrode (SCE) which was placed in a separate compartment maintained at room temperature. A platinum (Pt) spiral wire was used as the counter electrode (CE). The electrochemistry of the deposition solutions, both with and without CdCl₂ additive, was studied by cyclic voltammetry on bare FTO in order to determine the optimal cathodic potentials for the growth process. Electrodeposition was carried out potentiostatically at -1.0 V using an Autolab PGSTAT30 potentiostat/galvanostat and with rotation of WE (with constant speed of 300 rotations/min). The potentiostat was monitored by the AutoLab software. The growth parameters controlled during the electrodeposition procedure were the electrical potential, the electrical charge, and the cell temperature. The growth process ended in 150 or 120 min for pure ZnO or Cd–ZnO samples, respectively. After ECD, the layers were subsequently rinsed with DI water and dried in air to remove chloride salts and unreacted products from the surface. Samples were subjected to thermal annealing in air at 300 °C for 11 h taking into account that it may cause lattice relaxation and recoordination of the Cd alloy, leading to a desirable condition for alloying or doping.

Zn_{1-x}Cd_xO NWs were also electrodeposited on 3-μm-thick (0001)-oriented p-GaN:Mg layers supported on sapphire (from TDI Inc. Corp.) at -1.2 V and 85 °C from solutions containing

2, 6, and 8 μM CdCl₂. The details about ECD of ZnO NWs on p-GaN (0001) substrate have been given in our previous work.^{7,8} After electrodeposition, the samples were rinsed with DI water and then annealed at 300 °C for 10 h in air. In our experiments we prepared four sets of LED structures: #1 (pure ZnO NWs), #2, #3 and #4, ZnO NWs grown from baths containing 0, 2, 6, and 8 μM CdCl₂ in electrolyte, respectively.

Scanning electron microscopy (SEM) images were obtained with an Ultra 55 Zeiss FEG at an acceleration voltage of 10 kV. Quantitative elemental analyses (EDX) were realized with a Bruker Li-drift silicon detector. The layer structures were characterized with a high-resolution X-ray diffractometer (Siemens D5000) operated at 40 kV and 45 mA using Cu K α radiation with $\lambda = 1.5406 \text{ \AA}$ and a rotating sample holder. XRD patterns were measured between 10 and 90° with a scanning step of 0.02. Raman scattering was measured at room temperature with a Horiba Jobin Yvon LabRam IR system in a backscattering configuration. The 632.8 nm line of a He–Ne laser was used for off-resonance excitation with less than 4 mW power at the sample. The total transmittance studies at room temperature were made with unpolarized light at normal incidence in the wavelength range from 300 to 2100 nm using Cary 5000 (Varian) UV-vis-NIR spectrophotometer equipped with an integrating sphere. The photoluminescence (PL) was measured at room temperature according to a procedure described in a previous report.²⁷ The device electroluminescence was collected by an optical fiber connected to a CCD Roper Scientific detector (cooled Pixis 100 camera) coupled with a SpectraPro 2150i monochromator. The monochromator focal lens was 150 mm, grating of 300 grooves/mm blazed at 500 nm in order to record the emission of the ZnO in the whole near-UV-visible range.

2.2. Computational Section. Periodic calculations were carried out at the DFT level with the ab initio CRYSTAL09 code,²⁸ making use of localized (Gaussian) basis sets and solving self-consistently Hartree–Fock and Kohn–Sham equations thus allowing the efficient use of hybrid functionals for band structure calculations. These calculations were performed at DFT level applying the hybrid exchange correlation functional PBE0.²⁹ Durand and Barthelat large core pseudopotential with (31/31) contractions have been used on O atoms while large core Hay and Wadt pseudopotentials with (111/111/41) contraction and the all electron basis set (9-7-6-311-D631G20) have been considered for Zn and Cd atoms, respectively. This level of theory has already proven to provide reliable geometrical and electronic properties of ZnO based systems.²⁹ The wurtzite structure of ZnO was considered for calculations. Cd doping was investigated by substituting one zinc atom by one cadmium atom in $2 \times 2 \times 2$, $2 \times 2 \times 1$ and $2 \times 1 \times 1$ supercells, thus achieving a Cd concentration of 6.2, 12.5, and 25 mol %, respectively (Figure S1, Supporting Information). Comparisons will be performed between the Cd-doped ZnO and the bare ZnO systems. Sampling of the irreducible Brillouin zone was done with 28 k-points for the primitive cell (i.e., $1 \times 1 \times 1$ cell) and 10 k-points for the supercells. During structural optimizations, both of the atomic positions and cell parameters were free to relax.

3. RESULTS AND DISCUSSION

3.1. Electrochemical Deposition. Figure 1a shows typical cyclic voltammograms (CVs) of the real FTO–electrolyte interface recorded during the first voltammetric scan started at the rest potential on the bare FTO electrode. When both zinc and oxygen

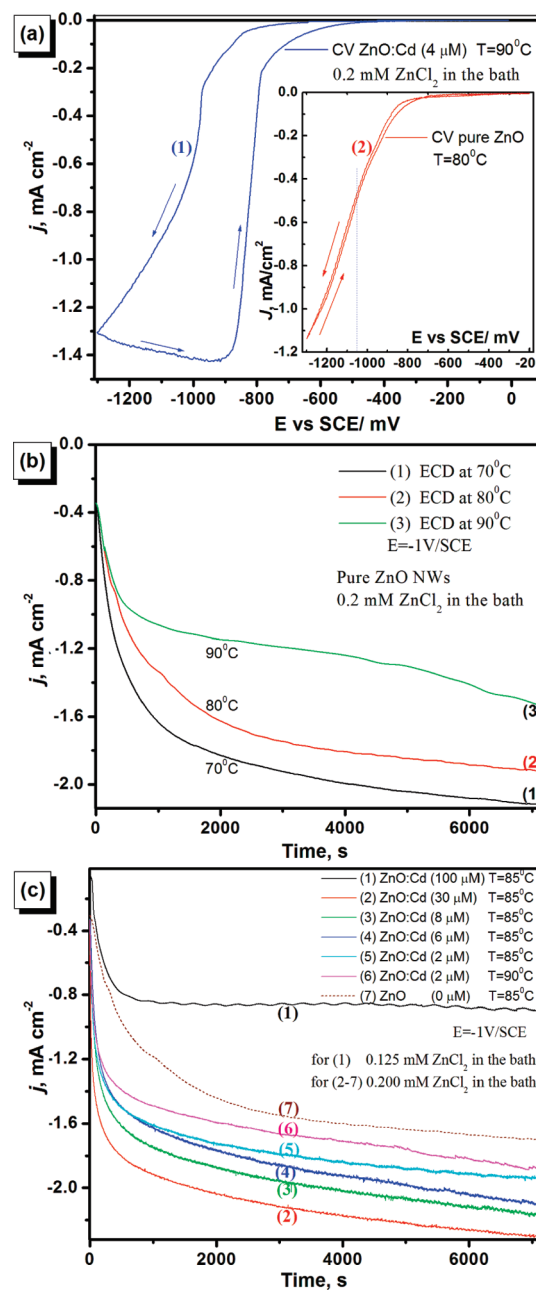


Figure 1. (a) Cyclic voltammograms recorded in bath containing 0.2 mM ZnCl₂ in 0.1 M KCl for pure ZnO (curve 2, inset in (a)) deposited at 80 °C and Zn_{1-x}Cd_xO (4 μM CdCl₂ in the electrolyte) (curve 1) at 90 °C. (b) Growth curves 1, 2, and 3 for pure ZnO NWs ECD at 70, 80, and 90 °C, respectively. (c) Current transient curves recorded upon sample growth at -1.0 V from 0.2 mM ZnCl₂ in 0.1 M KCl and different concentrations of CdCl₂ in the electrolyte. The meanings of the lines are shown in the inset. Scan rate 100 $\text{mV} \cdot \text{s}^{-1}$, $T = 85^\circ\text{C}$ and for curve 6, $T = 90^\circ\text{C}$.

are present in the electrolyte, we can observe in Figure 1a (inset, curve 2) a cathodic wave starting at -850 mV versus SCE with a maximum current density of 1.12 $\text{mA} \cdot \text{cm}^{-2}$ at -1.25 V (vs SCE) which can be assigned to the electrochemical reduction of molecular oxygen.^{30,31} The reverse scan current decreases rapidly for pure ZnO (see Figure 1a, curve 2 in inset). In the case of the solution containing 4 μM Cd(II), the presence of a diffusion

plateau extending from -1.25 to -0.9 V (curve 1, Figure 1a) is observed on the positive-going scan, then it starts to decrease rapidly (see curve 1 in Figure 1a). Afterward, the reverse scan current levels off (curve 1, Figure 1a). The curves indicate that the Cd-containing deposit has a higher electrocatalytic behavior for molecular oxygen reduction compared to pure ZnO. Similarly shaped curves (not shown to avoid repetition and superposition) for the cathodic scans were obtained with CdCl_2 concentration of $2\text{--}8 \mu\text{M}$ in the bath. From Figure 1a, the window between -0.85 and -1.25 V (vs SCE) is suitable for pure and Cd-doped ZnO formation. However, it has to be considered from previous observations³² that highly cathodic potentials (more negative) produce less dopant content in the resulting ZnO nanowires (assuming the same dopant concentration in the growth solution). This phenomenon has been observed previously in electrochemically grown ZnO doped with B and In.^{33,34} From the experimental electrochemical study of the system, a deposition potential of -1.0 V was chosen for the synthesis of pure and Cd-alloyed ZnO NWs.

In order to correlate the effects of bath temperature, current density, and aspect ratio of NWs/NRs, ECDs of pure ZnO and Cd-alloyed ZnO at different electrochemical bath temperatures were performed. Figure 1b shows the current transient recorded at -1 V/SCE upon pure ZnO NRs/NWs deposition on the FTO substrate at 70 , 80 , and 90 °C, with a rotation speed of 300 rpm of the WE. The illustrated curves 1–3 (Figure 1b) confirm that the pure ZnO NRs/NWs are excellent electrical conductors because the current density collected at the electrode is about -1.1 , -1.3 , and $-1.7 \text{ mA}\cdot\text{cm}^{-2}$ after 1000 s of ECD, respectively. It can be observed that the deposition current density is reduced by increasing the bath temperature. In Figure 1c, the current density significantly increased with increasing concentration of CdCl_2 in the electrolytes. This is important to clarify since we found a significant increase in current density by increasing dopant concentrations of CdCl_2 in the electrolytes (Figure 1c). Thomas and Cui,³² observed that a high concentration of Ag-dopant ions in the ECD growth solution disturbs regular growth of ZnO nanowire formation making the growth of high-quality and oriented NWs very difficult.

To produce high aspect ratio $\text{Zn}_{1-x}\text{Cd}_x\text{O}$ NRs/NWs on FTO, a growth temperature range of $85\text{--}90$ °C was selected. Figure 1c shows the current transient recorded at -1 V/SCE upon low-dimensional structure deposition on FTO substrate at about 85 °C and 90 °C in baths containing different concentrations of CdCl_2 and ZnCl_2 . The current density collected at the electrode is at about -1.15 , -1.59 , -1.61 , -1.75 , and $-1.95 \text{ mA}\cdot\text{cm}^{-2}$ after 1000 s of growth for ZnO baths containing 0 , 2 , 4 , 6 , and $8 \mu\text{M}$ CdCl_2 , respectively. The growth current density is clearly increased with increasing concentration of CdCl_2 in the bath. According to our previous observations in Figure 1b, we can reduce the current density by increasing the bath temperature. Curve 6 (Figure 1c) shows ECD growth of ZnO at $T = 90$ °C and a lower current density. It has been shown previously that the bath temperature influences the growth of pure ZnO NWs,³⁵ and this has been confirmed here for $\text{Zn}_{1-x}\text{Cd}_x\text{O}$ NWs grown from baths containing CdCl_2 and ZnCl_2 .

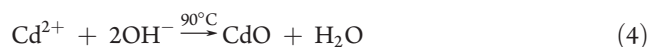
Fundamental physicochemical properties of cathodic ZnO films and nanowire synthesis in aqueous solutions of $[\text{ZnCl}_2] = 5.0$ and 0.2 mM , respectively, have been described previously.^{30,31} The electrodeposition of ZnO NRs/NWs is based on the electrochemical reaction involving oxygen, which electrochemically generates OH^- leading to the direct precipitation of zinc oxide on the FTO surface if the bath temperature is high enough.³⁶

In our case, the possible reactions for the ZnO and $\text{Zn}_{1-x}\text{Cd}_x\text{O}$ formation are



$$\text{p}K_S^{\text{ZnO}} = 16.66$$

where $\text{p}K_S^{\text{ZnO}}$ is the ZnO solubility constant.³⁶ The anionic species Cl^- and OH^- are formed by dissolving zinc chloride in water and by electrochemical reduction of molecular oxygen, respectively. Afterward, Zn(II) ions combine with hydroxyl ions OH^- yielding ZnO at relatively low temperature (90 °C in the following). With the presence of Cd^{2+} in the electrolyte, we can write similarly



If the Cd(II) concentration is low in the bath, we can suppose that cadmium will substitute zinc in the crystallographic lattice of the deposited host material. By increasing Cd(II) concentration in electrolyte the Cd thermodynamic solubility limits in ZnO can be reached.¹² The growth mechanism of pure ZnO NWs by electrodeposition was described in detail in a previous paper.³⁷

3.2. Morphological Studies. Panels a–c of Figure 2 show cross-sectional SEM images of pure ZnO NWs grown on FTO substrates at 70 , 80 , and 90 °C for 9000 s. On the basis of these SEM images, it can be concluded that sample ECD at 70 °C has a slower growth rate (even if the current density is higher, Figure 1b) than samples grown at 80 or 90 °C for the same duration (9000 s). This ECD regime (70 °C, -1 V) gives growth of large diameter and low-aspect ratio (length/diameter) NRs. The NR/NW aspect ratio increased significantly for samples grown at 80 °C and the SEM image in Figure 2c demonstrates that by increasing the temperature up to 90 °C, the layers were made of longer NWs with a higher aspect ratio in good agreement with a previous report by Pauperté et al.³⁸ The NW diameter in our samples was about 100 nm. Table 1 shows length/diameter ratio of NWs grown in different regimes. There is a marked increase in the aspect ratio of NRs from 3 to 4 to $16\text{--}19$ by increasing growth temperature, indicating that the aspect ratio strongly depends on the growth temperature, leading to controllable morphologies. Next, we performed ECD studies for ZnO baths containing $6 \mu\text{M}$ CdCl_2 in the same temperature range ($70\text{--}90$ °C). Figure 2d shows a top view of a ZnO layer grown on FTO substrate at 70 °C in an aqueous bath containing $6 \mu\text{M}$ CdCl_2 . When compared to pure ZnO NRs (Figure 2a), the rods shown in Figure 2d are better crystallized with better-defined edges. In this case, micro/nanorods with a low-aspect ratio can be seen (Figure 2d and Table 1). Figure 2e shows a cross-sectional view of $6 \mu\text{M}$ CdCl_2 –ZnO NWs/FTO grown at (80 °C), which show an increase in aspect ratio to 15 (Table 1). Figure 2f depicts the SEM image of $\text{Zn}_{1-x}\text{Cd}_x\text{O}$ ($6 \mu\text{M}$ CdCl_2) NWs on a FTO substrate grown at 90 °C. From Figure 2f it can be concluded that $\text{Zn}_{1-x}\text{Cd}_x\text{O}$ NWs have a higher aspect ratio (>30) than samples grown at lower temperatures (~ 15) (see Table 1) and that the presence of Cd(II) in the bath favors growth along the *c* axis. Figure 2f shows NWs with more uniform diameter distribution and shape if compared with pure ZnO

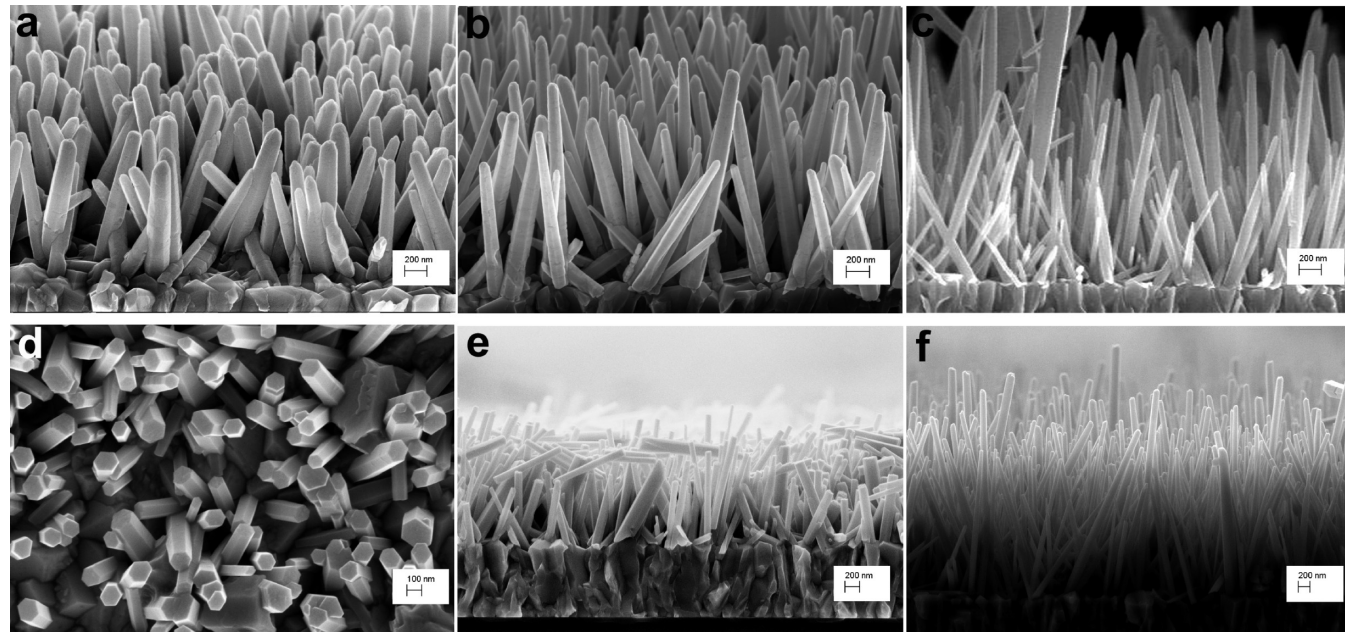


Figure 2. Effect of temperature and of dopant Cd(II) on aspect ratio of ZnO and $Zn_{1-x}Cd_xO$ low-dimensional structures. SEM micrographs (side views, except for panel d) of the layers electrodeposited on FTO substrate: (a) pure ZnO grown at 70 °C; (b) pure ZnO NWs grown at 80 °C; (c) pure ZnO NWs grown at 90 °C; (d) top view of $Zn_{1-x}Cd_xO$ ECD at 70 °C, 6 μM CdCl₂; (e) side view of $Zn_{1-x}Cd_xO$ ECD at 80 °C, 6 μM CdCl₂; and (f) side view of $Zn_{1-x}Cd_xO$ NWs ECD at 90 °C, 6 μM CdCl₂ in the electrolyte. ECD durations for (a–c) were 9000 s and for (d–f) were 7200 s.

Table 1. Aspect Ratios (Length/Diameter) of ZnO and $Zn_{1-x}Cd_xO$ NWs Electrodeposited on FTO Substrate

pure ZnO ECD at 70 °C, 9000 s	pure ZnO ECD at 80 °C, 9000 s	pure ZnO ECD at 90 °C, 9000 s	$Zn_{1-x}Cd_xO$ at 90 °C 2 μM CdCl ₂ , 7200 s	$Zn_{1-x}Cd_xO$ at 90 °C 4 μM CdCl ₂ , 7200 s	$Zn_{1-x}Cd_xO$ at 80 °C 6 μM CdCl ₂ , 7200 s	$Zn_{1-x}Cd_xO$ at 90 °C 6 μM CdCl ₂ , 7200 s
~3–4	~13–14	~16–19	~22–23	~24–26	~14–16	~29–31

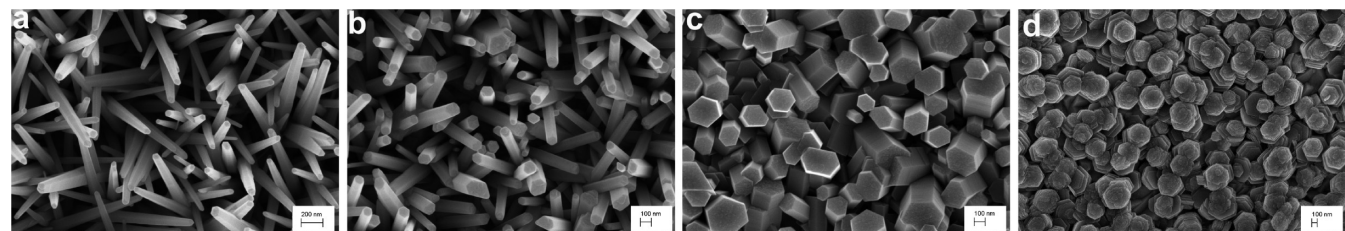


Figure 3. Effect of Cd concentration in the electrolyte on the material morphology. SEM micrographs (top view) of the low-dimensional ZnO structures electrodeposited on FTO substrate at 85 °C, $U = -1$ V: (a) $Zn_{1-x}Cd_xO$ (6 μM CdCl₂); (b) $Zn_{1-x}Cd_xO$ (10 μM CdCl₂); (c) $Zn_{1-x}Cd_xO$ (30 μM CdCl₂); (d) $Zn_{1-x}Cd_xO$ (100 μM CdCl₂). For (d), [ZnCl₂] in the electrolyte was 0.125 mM, and for (a, c), it was 0.20 mM.

NWs ECD at 90 °C (Figure 2c). No essential differences (except length) in the SEM images are observed from $Zn_{1-x}Cd_xO$ (2 μM CdCl₂) and $Zn_{1-x}Cd_xO$ (6 μM CdCl₂) NWs electrodeposited on FTO substrates at 90 °C. These observations suggest that the crystal growth of high aspect ratio NWs is favored by adding CdCl₂ in the electrolyte. The morphologies for ZnO NWs were nearly the same before and after annealing, which is in agreement with previous reports for ZnO.²⁷

On the basis of the results shown in Figure 2f and Table 1, we can conclude that high-aspect ratio NWs with a uniform diameter distribution can be electrodeposited at 90 °C in baths containing 6 μM CdCl₂ for 7200 s. The aspect ratio of $Zn_{1-x}Cd_xO$ NWs is higher by more than 50% versus pure ZnO ECD under same

growth conditions, even for longer durations of ECD. Also we found here that the growth of Cd–ZnO NWs becomes much faster with higher current densities compared to pure nanowires. The presence of Cd in the film favors the molecular oxygen reduction reaction and we can conclude that $Zn_{1-x}Cd_xO$ is a more electrocatalytic compound compared to pure ZnO.

We have next investigated the effect of Cd concentration in the bath on morphology (Figure 3, top views) of the low-dimensional ZnO structures electrodeposited on FTO substrates at 85 °C and -1 V vs SCE. Figure 3a shows $Zn_{1-x}Cd_xO$ NWs grown from an electrolyte containing 6 μM CdCl₂ and $j = -1.7 \text{ mA}\cdot\text{cm}^{-2}$. We have observed an increase of the aspect ratio of nanostructures with increasing Cd(II) concentration in the bath up to 6 μM

Table 2. $[CdCl_2]$ and $[Cd(II)]/[Zn(II)]$ in the Deposition Bath

sample	$[CdCl_2]$ (μM) in the deposition bath	$[Cd(II)]/[Zn(II)]$ in the deposition bath	x in the $Zn_{1-x}Cd_xO$ deposit ^a
1	0	0.00	0
2	2	0.01	0.053
3	4	0.02	0.116
4	6	0.03	0.131
5	10	0.05	0.204
6	30	0.15	0.269
7 ^b	100	0.794	0.435

^a Cadmium atomic % measured by EDX in the $Zn_{1-x}Cd_xO$ material deposited on FTO substrate. ^b 0.125 mM $ZnCl_2$ in the deposition bath.

$CdCl_2$ (Table 1). Such NWs (Figures 2f and 3a) are of interest for optoelectronic device applications as discussed above and for individual NW nanosensors, which will be discussed in future papers. For $6\text{--}8 \mu M$ $CdCl_2$ in the bath at $85^\circ C$, NWs with diameter <100 nm and the highest aspect ratio were deposited. With increase of $Cd(II)$ content to $10 \mu M$ $CdCl_2$ in the bath, NRs are formed with diameter in the range $80\text{--}120$ nm (see Figure 3b). Further increasing the $CdCl_2$ content to $30 \mu M$ in the electrolyte and using 0.2 mM $ZnCl_2$ yields microrods with well-shaped edges and diameters in the range $200\text{--}400$ nm (see Figure 3c). Figure 3d shows microdisks/microcylinder morphology of $Zn_{1-x}Cd_xO$ depositions grown by ECD in the bath containing $100 \mu M$ $CdCl_2$ and 0.125 mM $ZnCl_2$ at $85^\circ C$. The current density in this case was -0.8 mA cm^{-2} (Figure 1c, curve 1).

The values of x in $Zn_{1-x}Cd_xO$, measured by the EDX analyses, are presented in Table 2. It shows that the percentages of Cd in the deposited layers increase with the cadmium concentration in the electrolyte. However, for higher current density (more negative) a decrease in Cd content in ZnO deposited layers was observed (for the same Cd concentration in the electrolyte). In the experiment described by curve 1 in Figure 1c, ECD depositions had about 43.5 atom % Cd (sample 7 in Table 2). Figure 3d shows that, in this case, ECD produced microdisks/microcylinder morphology of the ZnO depositions. Due to the high Cd concentration in the film, the growth regime and the layer morphology are changed.

In the following section, we will focus on $Zn_{1-x}Cd_xO$ nanowires with high aspect ratio and then to $CdCl_2$ concentration in the deposition bath up to $8 \mu M$. Five sets of samples will be considered for further structural and optical characterizations, namely, (1) pure ZnO NWs and (2), (3), (4), and (5) which are $Zn_{1-x}Cd_xO$ NWs grown from baths containing 2, 4, 6, and $8 \mu M$ $CdCl_2$, respectively.

3.3. Structural Studies. Figure 4a,b shows the XRD patterns of pure ZnO and Cd-alloyed ZnO NWs with a high-aspect ratio. XRD studies of the crystal structure indicate only ZnO peaks in pure NWs (Figure 4a), along with the reflections from the FTO substrate. The pattern matches the lattice spacing of crystalline zinc oxide in the wurtzite structure (space group: $P6_3mc(186)$; $a = 0.3249 \text{ nm}$, $c = 0.5206 \text{ nm}$). The data closely match with the Joint Committee on Powder Diffraction Standards card for ZnO (JCPDS 036-1451). The XRD shows overexpression of the (002) plane suggesting preferential growth in the c direction perpendicular to the substrate for most of the NWs. These studies are in accordance with SEM observations (Figure 2). Figure 4b shows the XRD patterns of $6.0 \mu M$ Cd-alloyed ZnO nanowires, where CdO peaks are also present. Such CdO peaks were not detected for $CdCl_2$ concentration in the bath lower than

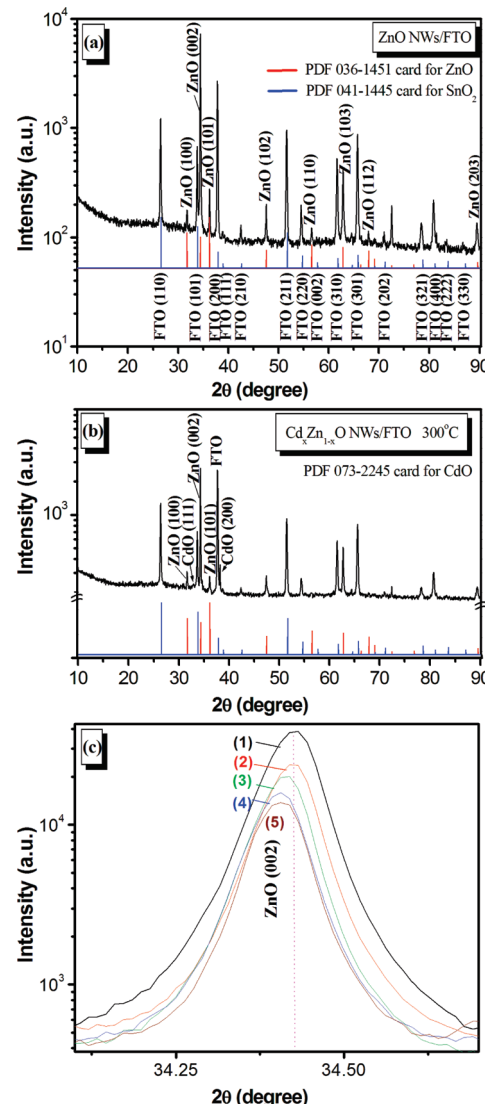


Figure 4. XRD patterns (a) of pure ZnO nanowires and (b) of $6.0 \mu M$ Cd-alloyed ZnO nanowires on FTO substrates. (c) Zoom of the (002) ZnO reflection peak. The meaning of the line for pure ZnO is (1), and for $Zn_{1-x}Cd_xO$ NWs the lines are (2) $2.0 \mu M$ $CdCl_2$, (3) $4.0 \mu M$ $CdCl_2$, (4) $6.0 \mu M$ $CdCl_2$, and (5) $8.0 \mu M$ $CdCl_2$ in the solution.

$6 \mu M$ are more pronounced in samples with x higher than ~ 0.13 . In all cases, wurtzite ZnO peaks were clearly found. This means that the dopant does not change the wurtzite structure of ZnO for low concentrations of $Cd(II)$ in the bath ($x < \sim 0.13$). At high $Cd(II)$ concentration ($x > \sim 0.13$), we have an admixture of Cd-doped ZnO and CdO . The fwhm of the $ZnO(002)$ peak changed from 0.109° (pure ZnO) to 0.085° ($6 \mu M$ Cd-ZnO) (Figure 2c and 2f). Figure 4c shows a slight shift of about 0.015° and 0.026° to lower 2θ values for the $ZnO(002)$ peak for $ZnO:Cd$ ($2 \mu M$) and $ZnO:Cd$ ($8 \mu M$) compared to pure ZnO (sample 1). This shift agrees with previous reports.^{21,41} It is suggested that the substitution of Zn (the ionic radius r of Zn^{2+} ($\sim 0.74 \text{ \AA}$)) by Cd (r of Cd^{2+} ($\sim 0.92 \text{ \AA}$)) takes place on the equivalent crystallographic positions of Zn in hexagonal wurtzite structures.²¹ From the XRD reported in Figure 4c, a slight lattice deformation/expansion was observed for Cd-ZnO NWs due to these differences in ionic radii.

Table 3. Computed Lattice Parameters and Band Gaps of Pure ZnO and $Zn_{1-x}Cd_xO$

	ZnO pure	Cd, 6.2%	Cd, 12.5%	Cd, 25.0%
a (Å)	3.330	3.356	3.378	3.446
c (Å)	5.172	5.203	5.235	5.225
Cd–O distance (Å) (002) direction/other directions	2.004	2.157/2.220	2.170/2.249	2.188/2.274
gap (eV)	3.94	3.84	3.72	3.35

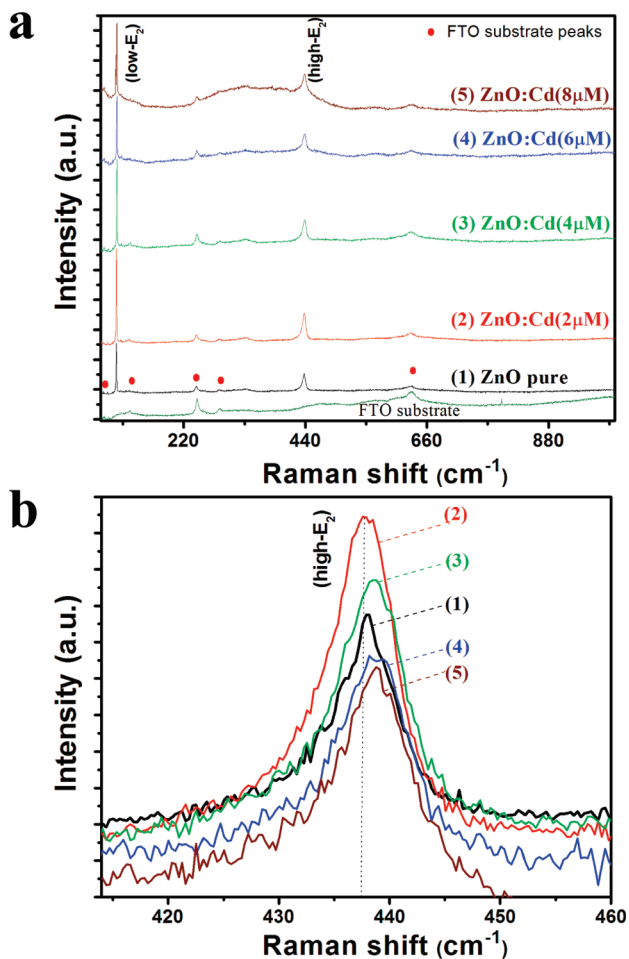


Figure 5. (a) Raman spectra of pure ZnO and $Zn_{1-x}Cd_xO$ NWs on FTO substrates. (b) High- E_2 mode of ZnO and $Zn_{1-x}Cd_xO$ NWs. Same line meanings as (a).

The lattice constants reported in the literature for bulk ZnO are $a = 3.249$ Å and $c = 5.206$ Å.²⁷ In our samples the lattice constants a and c of ZnO wurtzite structure were evaluated following the procedure reported in ref 27 and we obtained $a = 3.2506$ Å and $c = 5.2055$ Å for pure ZnO NWs. For concentrations of (2, 4, 6 μ M) Cd in the electrolyte, an increase in the ZnO lattice parameters a and c (3.2507 and 5.207 Å, respectively), was found. For higher concentration of Cd (8 μ M), a further increase in the lattice parameters of Cd-doped ZnO NWs, a and c (3.2507 and 5.209 Å, respectively) was measured.

Cell parameters have been calculed by DFT for various concentrations of Cd in the hexagonal crystal lattice of ZnO (Figure S1, Supporting Information) and the results are

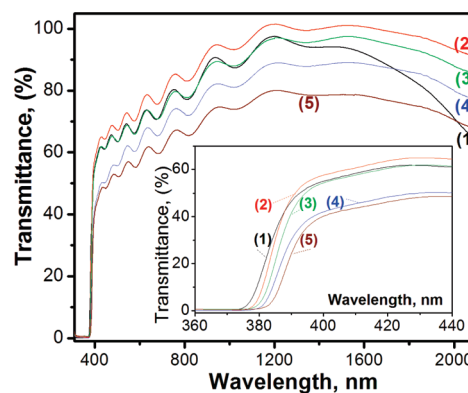


Figure 6. Variation of the total optical transmission curves ZnO and $Zn_{1-x}Cd_xO$ NWs ECD with four different concentrations of CdCl₂ in the bath. The inset is a zoom view of the band edge. Same line meanings as in Figure 4 and 5.

presented in Table 3. Clearly, the lattice parameters increase with increasing cadmium content. This is consistent with the larger cadmium atomic radius compared to the zinc atomic radius. In pure ZnO, Zn atoms have a tetrahedral coordination with a computed Zn–O distance of 2.004 Å. The Cd_{Zn} environment is no longer tetrahedral but a distorted tetrahedron with a Cd_{Zn}–O distance along the c axis longer than the three equivalent Cd–O distances in the other directions. Whatever the concentration of cadmium and the Cd–O bond chosen, the Cd–O distance is always larger than the Zn–O distance, also in agreement with the larger atomic radius of cadmium. There is thus a clear correlation between our experimental results and the computational studies on the expansion of the crystal lattice upon doping.

Pure and Cd-alloyed ZnO NWs were characterized by Raman spectroscopy. The E_2 (low) (100 cm⁻¹) mode in ZnO is associated with the vibration of heavy Zn sublattice and the E_2 (high) mode involves only the oxygen atoms. The E_2 (high) (438 cm⁻¹) mode is typical of the wurtzite phase material.⁵ Figure 5 shows clear Raman peaks indicating that different samples of pure ZnO and alloyed $Zn_{1-x}Cd_xO$ NWs on FTO exhibit similar scattering peaks, confirming that they have identical crystal wurtzite structures as demonstrated by XRD studies. For nanocrystalline or nanostructured materials, the crystalline Raman peak exhibits a frequency shift and peak broadening caused by the phonon confinement effect.⁴² Figure 5b shows the influence of Cd-alloying on the E_2 (high) mode of ZnO NWs. A slight shift is observed with increasing dopant concentration in ZnO NWs from 0 to 8 μ M. Moreover, as the Cd concentration in the bath increases from 6 to 8 μ M and above, the Raman line E_2 (high) mode broadens, which means that the crystallinity of ZnO decreases.²⁷ The frequency of the E_2 (high) mode (Figure 5b) of $Zn_{1-x}Cd_xO$ nanowires is higher than that of the standard value of 437 cm⁻¹ for bulk ZnO and slightly shifted with respect to pure ZnO NWs. This could be due to the stress increment of the nanowire top surface (002) because of the substitution of the smaller Zn atom by the larger Cd atom.⁴³ The relatively small shift suggests small stress in the ternary $Zn_{1-x}Cd_xO$ NWs compared with that of the ZnO NWs, which could be attributed to the stress relaxation effect in the nanorods.⁴³ At higher level of Cd alloying in ZnO a broad band between 250 and 400 cm⁻¹ appeared in curve 5 of Figure 5a. This band became more distinct for highly alloyed $Zn_{1-x}Cd_xO$ depositions (not shown).

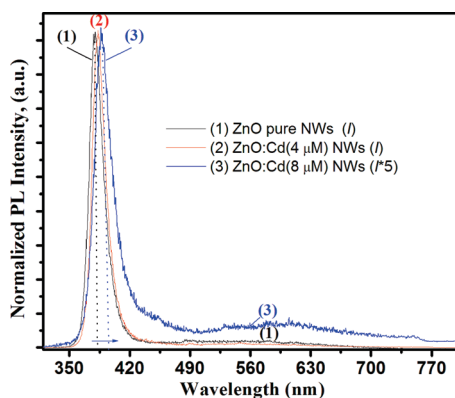


Figure 7. Photoluminescence spectra for pure and Cd-doped ZnO NWs with two different concentrations: curve 1, pure ZnO; 2, $Zn_{1-x}Cd_xO$ ($4 \mu M$ CdCl₂ in the bath); 3, $Zn_{1-x}Cd_xO$ ($8 \mu M$ CdCl₂ in the electrolyte bath).

4. OPTICAL PROPERTIES

The optical transmission spectra of undoped and Cd-alloyed ZnO NWs are shown in Figure 6. Pure ZnO and Cd (2 and 4 μM)-alloyed ZnO shows a transmittance higher than 60% in the visible region and it is higher than 90% in the near-infrared range. The observed interference fringes are due to the superimposition of waves that originate from the same point of the same source (a resonator being formed in the NWs). A transmission band-edge shift with increasing Cd content is clearly observed in the inset in Figure 6. The onset shift is due to a band gap narrowing of the material with increasing Cd content. In their study, Li et al.²¹ observed a gradual shift of the band gap from 3.37 to 3.25, 3.10, and 2.91 eV for x values of 0, 5, 9, and 15 atom % in $Zn_{1-x}Cd_xO$ alloys. In our experiment this shift is less marked but is in general agreement with previous works.^{20,22–24} The decrease in total optical transmittance with increasing Cd incorporation into ZnO NWs could be explained by possible appearance of more oxygen vacancies and Zn or Cd interstices, which lead to higher carrier concentration and accordingly to lower optical transmittance.²¹ Transparency of alloyed ZnO in the 1500–2100 nm interval (see Figure 6) decreases with increasing doping level, i.e., with an increasing concentration of free carriers in $Zn_{1-x}Cd_xO$ layers. Though this decrease of transparency is not significant, this means there is no sharp increase of reflectivity in the 1500–2100 nm range. In other words, we do not observe any metallic behavior characteristics of heavily doped TCO.^{44,45}

Photoluminescence characterization has been performed to investigate the optical quality and the emission properties of the electrodeposited layers. The spectrum for pure ZnO is dominated by the near band edge emission centered at 382 nm (curve 1, Figure 7). The negligible emission in the visible range is the signature of high-quality materials with a low intrinsic defect concentration. In the case of $Zn_{1-x}Cd_xO$ NWs, the main PL lines show a slight red shift relative to that of a pure ZnO NWs reference sample. The PL spectrum of higher alloyed $Zn_{1-x}Cd_xO$ NWs consists of two components as shown in curve 3 of Figure 7 and the intensity of the visible band increased with increasing doping. The near band-edge emission peak shifted to 384 and 387 nm after Cd doping in 4 and 8 μM CdCl₂ baths, respectively. From these studies, it can be concluded that the incorporation of Cd into ZnO material does not strongly shift

the E_g value. Our results are consistent with previous observations by Chikoidze et al.⁴⁴ Similarly, Wang et al.⁴⁶ observed a slight shift of the main UV peak in PL spectra by 6 and 9 nm from ZnO nanorods with Cd (6.2%) and Cd (7.6%), respectively. From Figure 7, curve 3, it can be seen that the emission intensity is markedly reduced for $Zn_{1-x}Cd_xO$ NWs and the full width at half-maxima of the UV peak is slightly broadened. This could be due to Cd content fluctuation, bound states related to unintentionally doped impurities or crystallographic defects, and/or strain-induced band gap modification.^{46–48} This phenomenon is frequently observed in doped semiconductors.

It is important to note that for values higher than 8 μM Cd in the bath, the intensity of PL emission decreased with increasing Cd concentration. In curve 3, Figure 7, the green-orange PL observed for higher Cd doping concentration indicates a slightly poorer crystal quality compared to pure ZnO nanorods and other $Zn_{1-x}Cd_xO$ NWs.^{49–51} The mechanism of such deep-trap emission of ZnO is still under discussion. Many sources of emission in the green region, such as oxygen vacancies, antisite oxygen, zinc vacancies or interstitials, impurities, or surface defects have been assigned to this emission.

In order to better understand our experimental observations, we have analyzed the electronic structures of three $Zn_{1-x}Cd_xO$ systems, with $x = 0.062, 0.125$, and 0.25 , and compared them to the bare ZnO structure. The geometry of each system was first optimized, and then the density of states (DOS) and band structures were computed (Figure 8). The calculated band gaps are reported in Table 3. From these calculations it appears that for x varying from 0 to 0.25, the band gap of the system is reduced by about 0.6 eV in good agreement with the computing results by Palacios et al.⁵² The discrepancies observed between the absolute values of computed and experimental band gap are in the range expected for DFT calculations. From the computed DOS and band structures, we can conclude that the band gap reduction is not due to the insertion of a band centered on cadmium inside the band gap. The behavior here is different from that found in the case of copper doping.⁵³ In the case of copper, replacing Zn atoms by Cu atoms in the ZnO lattice introduces new energy levels (Cu 3d orbitals) in the band gap, near the valence band and the conduction band which are responsible for the band gap narrowing. In the case of Cd, the variation is due to the decrease in the conduction band edge energy. We can note that the valence band edge is made of O 2p and Zn 3d orbitals and the conduction band edge is made of Zn 4s orbitals for each system. The calculations suggest that the gap reduction is due to the increase of cell parameters after the insertion of cadmium. In order to validate this assumption, we performed the optimization of a pure ZnO supercell, but imposing the cell parameters obtained with 25% of cadmium alloying. The DOS of this system is presented as a blue line in Figure 8a. The computed gap is 3.40 eV, a value which is very close to the calculated gap of the cadmium-doped ($x = 0.25$) system (3.35 eV) and which fully confirms the hypothesis.

5. APPLICATIONS TO LED STRUCTURES

In light of our previous work on ZnO NW based LEDs,^{7,8} we have explored the applicability of the n-type $Zn_{1-x}Cd_xO$ NWs as the light emitters in n- $Zn_{1-x}Cd_xO$ /p-GaN heterojunction LED structures. Figure 9b shows a cross-sectional view of

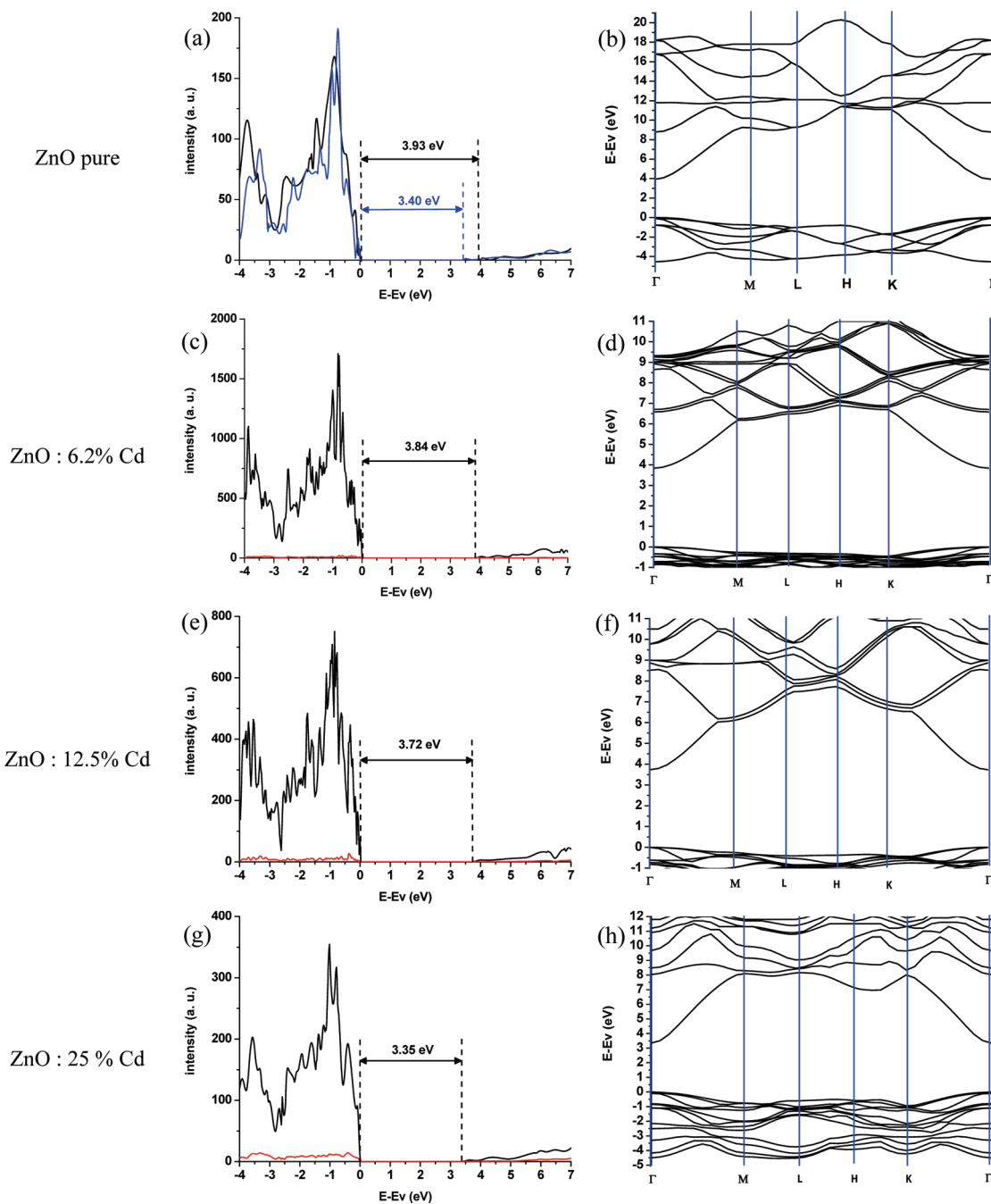


Figure 8. Computed density of states (DOS) and band structures of pure ZnO (a, b) and of Cd-alloyed ZnO with various Cd content (c–h). The blue line in (a) represents the DOS of pure ZnO with cell parameters calculated for $Zn_{0.75}Cd_{0.25}O$.

ZnO NWs/p-GaN substrate used in LED fabrication. Figure 9c is a schematic representation of the developed p–n heterojunction based LED structure ($(n\text{-}Zn_{1-x}\text{Cd}_x\text{O}/p\text{-GaN:Mg})/\text{sapphire/Cu}$).

The LED structure was forward biased at room temperature with a Keithley voltage source. The turn on voltage for the emission detection was 5 V. It was slightly larger for the LED structure based on $Zn_{1-x}\text{Cd}_x\text{O}$ NWs compared with pure ZnO-NWs/GaN (4.4 V). This may be due to the interface defects between ZnO:Cd and p-GaN and a higher contact resistance.

In Figure 9a, room-temperature electroluminescence (EL) spectra of the device structures made from $Zn_{1-x}\text{Cd}_x\text{O}$

nanowires (grown in 2, 6, 8 μM CdCl_2 in the bath) are presented and compared with those based on pure ZnO NWs/p-GaN used as reference (curve 1). In every case, a single short wavelength emission, red shifted toward the violet spectral range, is observed in Cd-doped ZnO. The appearance of the electroluminescence under forward bias of the LED structure and the wavelength shift of up to 24 nm with x provides insights that the $n\text{-}Zn_{1-x}\text{Cd}_x\text{O}$ nanostructures act as the light emitters in the devices. Moreover, the wavelength shift is more pronounced for EL than for PL. This suggests that the EL becomes a more interfacial process with Cd content, influenced by the band-edge offset of the heterojunction. We have clearly established that Cd doping is a powerful

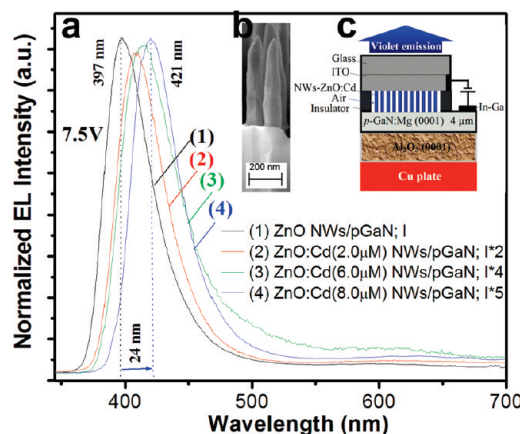


Figure 9. (a) Room-temperature electroluminescence spectra of n-ZnO/p-GaN:Mg and n-Zn_{1-x}Cd_xO/p-GaN:Mg NWs heterostructured LEDs under 7.5 V forward bias. (b) Cross-sectional SEM image of n-ZnO nanowires epitaxially grown by ECD on p-GaN:Mg. (c) LED device structure used in our studies.

means to tune the emission color by controlling the dopant concentration in Zn_{1-x}Cd_xO NWs.

6. CONCLUSIONS

In summary, quasi-vertically aligned high aspect ratio Zn_{1-x}Cd_xO nanowires were synthesized by electrochemistry on FTO substrate. The aspect ratio (>30) of nanostructures increased with increasing Cd(II) concentration in the bath up to 6 μM CdCl₂. The growth mechanism of the NWs has been presented and discussed in detail. Temperature and current density were shown to be the critical factors affecting the morphology of low-dimensional Zn_{1-x}Cd_xO structures. Structural changes have been observed by XRD and Raman studies which have been explained by the partial replacement of Zn atoms by Cd atoms in the lattice structure which was confirmed by a computational study. However, the doping has been observed for x < 0.13% in the wires whereas Zn_{1-x}Cd_xO was admixed with crystallized CdO for higher x.

The optical transmission band edge red shifted with increasing Cd content in the deposition bath due to a band gap narrowing of the material with the Cd content. It was found that the higher the concentration of cadmium in the electrolyte, the lower the band gap of the material. We have shown that the band gap reduction was not due to the appearance of new bands inside the band gap, as found in other systems,⁵³ but was due to the expansion of the lattice parameters.

A PL study has been performed to investigate the origin of EL emission and showed a red shift of the main emission lines relative to that of a pure ZnO NWs reference sample. Finally, LED structures have been fabricated and we have demonstrated the possibility to integrate electrodeposited Zn_{1-x}Cd_xO NWs in the device. A substantial red shift of EL peak position by 25 nm was obtained from the LED structure with Zn_{1-x}Cd_xO (8 μM CdCl₂ in the bath) NWs. Electrodeposition is shown to be a valuable technique in current effort to realize efficient, low-cost emitters based on Cd-doped ZnO for LEDs with adjustable emission wavelength.

■ ASSOCIATED CONTENT

5 Supporting Information. Optimized structure of Cd-doped ZnO (12.5% of Cd) of a 2 × 2 × 1 supercell and of a

4 × 4 × 2 supercell. This material is available free of charge via the Internet at <http://pubs.acs.org>.

■ AUTHOR INFORMATION

Corresponding Author

*E-mail: thierry-pauporté@chimie-paristech.fr; oleg-lupan@chimie-paristech.fr.

Notes

⁵On leave from: Department of Microelectronics and Semiconductor Devices, Technical University of Moldova, 168 Stefan cel Mare Blvd., Chisinau, MD-2004, Republic of Moldova.

■ ACKNOWLEDGMENT

This research was performed with the financial support of the C-nano Ile-de-France program (nanoZnO-LED Project). The authors are grateful to Dr. S. Delpech (LECIME-ENSCP) for access to the Raman spectrometer. Dr. O. Lupon acknowledges the CNRS for support as an invited scientist at the LECIME-Chimie-Paristech (France).

■ REFERENCES

- (1) Ozgur, U.; Alivov, Y. I.; Liu, C.; Teke, A.; Reshchikov, M. A.; Dogan, S.; Avrutin, V.; Cho, S. J.; Morkoc, H. *J. Appl. Phys.* **2005**, 98, 041301.
- (2) Gudiksen, M. S.; Lauhon, L. J.; Wang, J.; Smith, D. C.; Lieber, C. M. *Nature* **2002**, 415, 617.
- (3) Wang, X.; Li, Q.; Liu, Z.; Zhang, J.; Liu, Z.; Wang, R. *Appl. Phys. Lett.* **2004**, 84, 4941.
- (4) Zhong, J.; Chen, H.; Saraf, G.; Lu, Y.; Choi, C. K.; Song, J. J.; Mackie, D. M.; Shen, H. *Appl. Phys. Lett.* **2007**, 90, 203515.
- (5) Lupon, O.; Ursaki, V. V.; Chai, G.; Chow, L.; Emelchenko, G. A.; Tiginianu, I. M.; Gruzintsev, A. N.; Redkin, A. N. *Sens. Actuators, B* **2010**, 144, 56.
- (6) Lupon, O.; Guérin, V. M.; Tiginianu, I. M.; Ursaki, V. V.; Chow, L.; Heinrich, H.; Pauporté, T. *J. Photochem. Photobiol., A* **2010**, 211, 65–73.
- (7) Lupon, O.; Pauporté, T.; Viana, B. *Adv. Mater.* **2010**, 22, 3298–3302.
- (8) Lupon, O.; Pauporté, T.; Viana, B.; Tiginianu, I. M.; Ursaki, V. V.; Cortés, R. *ACS Appl. Mater. Interfaces* **2010**, 2, 2083.
- (9) Lupon, O.; Pauporté, T.; Viana, B. *J. Phys. Chem. C* **2010**, 114 (35), 14781–14785.
- (10) Law, J. B. K.; Thong, J. T. L. *Appl. Phys. Lett.* **2006**, 88, 133114.
- (11) Zhu, G.; Yang, R.; Wang, S.; Wang, Z. L. *Nano Lett.* **2010**, 10 (8), 3151–3155.
- (12) Schmidt-Mende, Lukas; MacManus-Driscoll, J. L. *Mater. Today* **2007**, 10, 40–48.
- (13) Von Wenckstern, H.; Schmidt, H.; Brandt, M.; Lajn, A.; Pickenhain, R.; Lorenz, M.; Grundmann, M.; Hofmann, D. M.; Polity, A.; Meyer, B. K.; Saal, H.; Binnewies, M.; Börger, A.; Becker, K.-D.; Tikhomirov, V. A.; Jug, K. *Prog. Solid State Chem.* **2009**, 37, 153–172.
- (14) Makino, T.; Segawa, Y.; Kawasaki, M.; Ohtomo, A.; Shiroki, R.; Tamura, K.; Yasuda, T.; Koinuma, H. *Appl. Phys. Lett.* **2001**, 78, 1237.
- (15) Wang, F.; Ye, Z.; Ma, D.; Zhu, L.; Zhuge, F. *J. Cryst. Growth* **2005**, 283, 373–377.
- (16) Zhou, S. M.; Zhang, X. H.; Meng, X. M.; Wu, S. K.; Lee, S. T. *Mater. Res. Bull.* **2006**, 41, 340–346.
- (17) Wang, Y. S.; John Thomas, P.; O'Brien, P. *J. Phys. Chem. B* **2006**, 110, 21412–21415.
- (18) Liu, J. Z.; Yan, P. X.; Yue, G. H.; Chang, J. B.; Zhuo, R. F.; Qu, D. M. *Mater. Lett.* **2006**, 60, 3122–3125.
- (19) Wan, Q.; Li, Q. H.; Chen, Y. J.; Wang, T. H.; He, X. L.; Gao, X. G.; Li, J. P. *Appl. Phys. Lett.* **2004**, 85, 3085.

- (20) Yogeeswaran, G.; Chenthamarakshan, C. R.; Seshadri, A.; de Tacconi, N. R.; Rajeshwar, K. *Thin Solid Films* **2006**, *515*, 2464.
- (21) Li, G. R.; Zhao, W. X.; Bu, Q.; Tong, Y. X. *Electrochem. Commun.* **2009**, *11*, 282.
- (22) Tortosa, M.; Mollar, M.; Mari, B. *J. Cryst. Growth* **2007**, *304*, 97–102.
- (23) Mari, B.; Tortosa, M.; Mollar, M.; Bosca, J. V.; Cui, H. N. *Opt. Mater.* **2010**, *32*, 1423–1426.
- (24) Chang, Y. S.; Chen, K. H. *J. Appl. Phys.* **2007**, *101*, 033502.
- (25) Pauporté, T.; Yoshida, T.; Cortès, R.; Froment, M.; Lincot, D. *J. Phys. Chem. B* **2003**, *107*, 10077.
- (26) Pauporté, T.; Bataille, G.; Joulaud, L.; Vermersch, J. F. *J. Phys. Chem. C* **2010**, *114*, 194–202.
- (27) Lupan, O.; Pauporté, T.; Chow, L.; Viana, B.; Pellé, F.; Roldan Cuanya, B.; Ono, L. K.; Heinrich, H. *Appl. Surf. Sci.* **2010**, *256*, 1895.
- (28) Saunders, V. R.; Dovesi, R.; Roetti, C.; Orlando, R.; Zicovich-Wilson, C. M.; Harrison, N. M.; Doll, K.; Civalleri, B.; Bush, I.; D'Arco, Ph.; Llunell, M. *Crystal 09 User's Manual*; Universita di Torino: Torino, Italy, 2009.
- (29) Adamo, C.; Barone, V. *J. Chem. Phys.* **1999**, *110*, 6158.
- (30) Peulon, S.; Lincot, D. *J. Electrochem. Soc.* **1998**, *145*, 864.
- (31) Goux, A.; Pauporté, T.; Lincot, D. *Electrochim. Acta* **2006**, *51*, 3168–3172.
- (32) Thomas, M. A.; Cui, J. B. *J. Phys. Chem. Lett.* **2010**, *1*, 1090–1094.
- (33) Ishizaki, H.; Imaizumi, M.; Matsuda, S.; Izaki, M.; Ito, T. *Thin Solid Films* **2002**, *411*, 65–68.
- (34) Machado, G.; Guerra, D. N.; Lienen, D.; Ramos-Barrado, J. R.; Marotti, R. E.; Dalchiele, E. A. *Thin Solid Films* **2005**, *490*, 124–131.
- (35) Pauporté, T.; Jouanno, E.; Pellé, F.; Viana, B.; Aschehoug, P. *J. Phys. Chem. C* **2009**, *113*, 10422–10431.
- (36) Goux, A.; Pauporté, T.; Chivot, J.; Lincot, D. *Electrochim. Acta* **2005**, *50*, 2239–2248.
- (37) El Belghiti, H.; Pauporté, T.; Lincot, D. *Phys. Status Solidi A* **2008**, *205*, 2360–2364.
- (38) Harada, J.; Ohshima, K. *Surf. Sci.* **1981**, *106*, 51.
- (39) Matsubara, T.; Iwase, Y.; Momokita, A. *Prog. Theor. Phys.* **1977**, *58*, 1102.
- (40) Yasuda, H.; Mori, H. *J. Cryst. Growth* **2002**, *237*, 234.
- (41) Vigil, O.; Vaollant, L.; Cruz, F.; Santana, G.; Moroles-Acevedo, A.; Contreras-Puente, G. *Thin Solid Films* **2000**, *361*, 53.
- (42) Richter, H.; Wang, Z. P.; Ley, L. *Solid State Commun.* **1981**, *39*, 625.
- (43) Wang, F.; He, H.; Ye, Z.; Zhu, L.; Tang, H.; Zhang, Y. *J. Phys. D: Appl. Phys.* **2005**, *38*, 2919–2922.
- (44) Chikoidze, E.; Nolan, M.; Modreanu, M.; Sallet, V.; Galtier, P. *Thin Solid Films* **2008**, *516*, 8146–8149.
- (45) Hamberg, J.; Granqvist, C. G. *J. Appl. Phys.* **1986**, *60*, R123.
- (46) Wang, F. Z.; Ye, Z. Z.; Ma, D. W.; Zhu, L. P.; Zhuge, F.; He, H. P. *Appl. Phys. Lett.* **2005**, *87*, 143101.
- (47) Park, W. I.; Yi, G. C.; Jang, H. M. *Appl. Phys. Lett.* **2001**, *79*, 2022.
- (48) Ohtomoa, A.; Kawasaki, M.; Ohkubo, I.; Koinuma, H.; Yasuda, T.; Segawa, Y. *Appl. Phys. Lett.* **1999**, *75*, 980.
- (49) Dai, Y.; Zhang, Y.; Li, Q. K.; Nan, C. W. *Chem. Phys. Lett.* **2002**, *83*, 358.
- (50) Vanheusden, K.; Warren, W. L.; Seager, C. H.; Tallant, D. R.; Voigt, J. A.; Gnade, B. E. *J. Appl. Phys.* **1996**, *79*, 7983.
- (51) Egehaaf, H. J.; OelKrug, D. *J. Cryst. Growth* **1996**, *161*, 190.
- (52) Palacios, P.; Aguilera, I.; Wahnon, P. *Thin Solid Films* **2010**, *518*, 4568–4571.
- (53) Lupan, O.; Pauporté, T.; Le Bahers, T.; Viana, B.; Ciofini, I. *Adv. Funct. Mater.* **2011**, DOI: 10.1002/adfm.201100258.